Targeted Photothermal Therapy of Melanoma in C57BL/6 Mice using Fe$_3$O$_4$@Au Core-shell Nanoparticles and Near-infrared Laser

Pandesh S.[1], Haghjooy Javanmard Sh.[2], Shakeri-Zadeh A.[3], Shokrani P.[1]*

ABSTRACT

Background: Gold nanoshells can be tuned to absorb a particular wavelength of light. As a result, these tunable nanoparticles (NPs) can efficiently absorb light and convert it to heat. This phenomenon can be used for cancer treatment known as photothermal therapy. In this study, we synthesized Fe$_3$O$_4$@Au core-shell NPs, magnetically targeted them towards tumor, and used them for photothermal therapy of cancer.

Objective: The main purpose of this research was to synthesize Fe$_3$O$_4$@Au core-shell NPs, magnetically target them towards tumor, and use them for photothermal therapy of cancer.

Material and Methods: In this experimental study, twenty mice received 2×10^6 B16-F10 melanoma cells subcutaneously. After tumors volume reached 100 mm^3, the mice were divided into five groups including a control group, NPs group, laser irradiation group, NPs + laser group and NPs + magnet + laser group. NPs were injected intravenously. After 6 hours, the tumor region was irradiated by laser (808 nm, 2.5 W/cm^2, 6 minutes). The tumor volumes were measured every other day.

Results: The effective diameter of Fe$_3$O$_4$@Au NPs was approximately 37.8 nm. The average tumor volume in control group, NPs group, laser irradiation group, NPs + laser irradiation group and NPs + magnet + laser irradiation group increased to 47.3, 45.3, 32.8, 19.9 and 7.7 times, respectively in 2 weeks. No obvious change in the average body weight for different groups occurred.

Conclusion: Results demonstrated that magnetically targeted nano-photothermal therapy of cancer described in this paper holds great promise for the selective destruction of tumors.

Introduction

Melanoma has become a major global public health concern. Over the last years, the frequency of melanoma new cases in Western countries has risen quickly, and this disease has become one of fatal cancers [1, 2]. Hyperthermia is one of the most important cancer treatment methods [3]. Hyperthermia is usually defined as heating of a tissue to temperature ranges from 42 to 50 °C [4-6]. For the destruction of a tumor, various thermal energy delivery meth-

[1]PhD, Department of Medical Physics, School of Medicine, Isfahan University of Medical Sciences, Isfahan, Iran
[2]PhD, Applied Physiology Research Center, Cardiovascular Research Institute, Isfahan University of Medical Sciences, Isfahan, Iran
[3]PhD, Department of Medical Physics, School of Medicine, Iran University of Medical Sciences, Tehran, Iran

*Corresponding author:
P. Shokrani
Department of Medical Physics, School of Medicine, Isfahan University of Medical Sciences, Isfahan, Iran
E-mail: shokrani@med.mui.ac.ir

ods including microwave, radiofrequency, focused ultrasound and laser have been developed [7-9]. Hyperthermia therapy using laser beams is one of the current tools to fight cancer [4, 10, 11]. Photothermal therapy (PTT) is a minimally invasive therapy that typically involves the usage of photothermal agents and laser light [12, 13]. Generally, for minimizing laser absorption in other tissues and for increasing laser penetration, near-infrared (NIR) wavelengths around 650-900 nm are used [9]. Metal NPs absorb laser light and act as photothermal agents because of their enhanced absorption cross sections [6]. Advantages of gold nanoparticles (Au NPs) in PTT include a strong light absorption cross section of Au NPs (due to surface plasmon resonance), and biocompatibility, and ease of linking of Auto proteins and antibodies [14, 15]. Three major shapes of Au NPs used in PTT include spheres, rods and core-shells. Gold nanoshells generally consist of a silica core and a thin gold shell. In addition to silica, different cores have been used to take advantage of such a nanomaterial [16, 17]. For example, Fe_3O_4@Au core-shell is used to produce multifunctional NPs [18-21]. Advantages of Fe_3O_4@Au NP as a multifunctional nanoparticle include its strong absorption cross section due to the presence of Au as a photothermal agent, the ability of such a nanomaterial as a contrast agent in both CT scan and MRI modalities and its capability to be used in the magnetic targeting of a tumor [18, 21-23]. By adjusting the core diameter and shell thickness, the absorption peak of Fe_3O_4@Au NPs can be tuned to NIR region [6, 17]. In this study, Fe_3O_4@Au NPs were synthesized and characterized using transmission electron microscopy (TEM), dynamic laser light scattering (DLS) and UV-vis spectrophotometer. Thereafter, Fe_3O_4@Au NPs were exposed to a continuous-wave (CW) diode laser at a wavelength of 808 nm to assess the photothermal effect of the NPs. Finally, this nanostructure was used for magnetically targeted photothermal therapy in mice bearing melanoma tumor.

For this purpose, after intravenous injection of Fe_3O_4@Au NPs, they were accumulated in tumor region using a 3500 Gauss magnet, and then tumor site was irradiated with laser beam.

Material and Methods

This study is an experimental study. Material and methods that was used in this study was as follow.

Chemicals

Iron (III) chloride hexahydrate (>99%), iron (II) chloride tetrahydrate (>99%), methanol (99.9%), ammonia (32%) and toluene (>99%) were purchased from Merck. 3-Amino-propyltrimethoxysilane (97%) and Gold (III) chloride solution were purchased from Fluka and Sigma, respectively.

Fe_3O_4@Au Core-shell NPs Synthesis

Fe_3O_4@Au core-shell NPs were synthesized according to the method recently published by Montazerabadi et al, [24]. Briefly, Fe_3O_4@Au NPs were synthesized using an alteration of the co-precipitation technique of Massart [25]. First, 12.5 mL of NH_3 (2 M) was added drop wise to a 2:1 solution of $FeCl_3.6H_2O$ and $FeCl_2.4H_2O$ under mechanical stirring. When the addition was augmented, the sediment was isolated by an external magnet, washed three times with methanol, diffused in 50 mL of toluene and kept as the source of Fe_3O_4 colloidal solution. Then, 3-Aminopropyl trimethoxysilane (APTMS) (25 µL) was added to 12.5 mL of Fe_3O_4 NPs and sonicated for 30 minutes. The solution then was heated at 60 °C for 4 hours in an oven. The sediment was separated with a magnet, washed three times with methanol to eliminate extra toluene and APTMS, and then dispersed in methanol.

To form Au shells on the surface of Fe_3O_4 NPs, Au NPs with a diameter of 3.5 nm were synthesized as detailed in the literature [26] and immobilized onto the surface of APTMS-functionalized Fe_3O_4 NPs. In this regard, 4 mL of APTMS-functionalized Fe_3O_4 NPs (51.5

mM Fe) in methanol was added drop wise to a 25 mL solution of undiluted Au NPs (0.198 mM Au). Next, 4mL of methanol and 10mL of water were added to maximize the coverage of Au NPs on the surface of Fe_3O_4 NPs. After 2 hours of stirring at room temperature, Au NPs were immobilized onto the surface of Fe_3O_4 NPs. The resulting NPs were separated with an external magnet, washed three times with deionized water and dispersed in 15 mL of deionized water. At the end, 0.011 g of chloroauric acid was added to 15mL of a prepared solution of Au immobilized on the surface of Fe_3O_4 NPs under sonication. To finalize shell formation, 0.4 mL (78.9 mM) of ascorbic acid was added to the final solution. After 2 hours of incubation, a contiguous and complete Au shell was constructed on the surface of Fe_3O_4 NPs.

Characterization Methods

Before any use in experimental tests, Fe_3O_4@Au NPs were characterized. Zeiss LEO 906 transmission electron microscope (TEM) was used for analyzing the morphological characteristics of NPs. In this regard, NPs were suspended in deionized water and sonicated for 10 minutes. A small drop of suspension was mounted onto a carbon-coated copper grid and allowed to vaporize. Thereafter, the thoroughly dried grid was observed under a transmission electron microscope at 120 KV. Furthermore, the hydrodynamic size distribution of NPs was determined using dynamic laser light scattering (DLS) with a Malvern Zetasizer, NANO ZS (Malvern Instruments Limited, UK). UV-visible (UV-vis) absorption spectrophotometric measurements were performed by a single-beam UV-vis spectrometer, Agilent 8453, using quartz cells of 1 cm path length and DI water as the reference at room temperature.

Photothermal Conversion of Fe_3O_4@Au NPs Solutions

Representative samples with 0 µg/mL, 12.5 µg/mL, 25 µg/mL, 37.5 µg/mL and 50 µg/mL of Fe_3O_4@Au NPs in 300 µL deionized water were pelleted in a 96-well cell culture plate. A home-built 808 nm continuous wave diode laser was used as a light source. Samples at each Fe_3O_4@Au NPs concentration were irradiated with power densities of 0.9 W/cm^2, 1.8 W/cm^2, 2.5 W/cm^2 and 3.5 W/cm^2. Temperature variation was determined using a thermocouple probe Type K with measurements recorded at 30-second intervals. The temperature measurements were performed using a thermometer model ST 8891E manufactured by Standard Instruments Co. (China). The thermocouple probe was placed vertically at the center of each sample. The initial temperatures of samples were recorded for the first 10 seconds before irradiation of the NIR laser; each sample was then irradiated for 360 seconds, and temperature variation curves were plotted.

Cell Culture and Tumor Induction

Cell Line

Mouse malignant melanoma cell line B16/F10 (C540) which can grow in C57BL/6 strain mouse was purchased from the National Cell Bank of Iran (NCBI, Pasteur Institute of Iran). The cells were cultured in Dulbecco's Modified Eagle's Medium (DMEM) supplemented with 4 mM L-glutamine, 4.5 g/l glucose, 10% fetal bovine serum (FBS) and antibiotics (100 µg/ml streptomycin and 100 µg/ml penicillin). The cells were maintained in culture flasks at 37°C in a humidified incubator containing 5% CO_2. When the confluency of melanoma cells reached 80%, the cells were washed with phosphate buffer saline (PBS) and detached from the bottom of the flask with PBS containing 0.25% trypsin and 0.03% EDTA, and then pelleted by brief centrifugation. The supernatant was removed, cell pellets were resuspended in PBS, and the cell was counted.

Animals

Male C57BL/6 mice, at age of 4-6 weeks (20-25 gr) obtained from Pasteur Institute of Iran were used for in-vivo experiments. The

mice were housed in a light controlled house at 25°C and humidity of 55% with free access to water and food. All animal procedures were performed in adaptation with the protocol constructed by the committee of an animal study in Isfahan University of Medical Sciences. A 12/12 dark/lightcycle was followed as mentioned in the animal vivarium.

Twenty male C57BL/6 mice were chosen to serve as recipient mice for tumor inoculation. Mice were maintained for 1 week to acclimate to the environment before the experiment. C57BL/6 mice were implanted with 2×10^6 B16-F10 melanoma cells in 100 μL of PBS subcutaneously in the right flank using a disposable tuberculin syringe. Primary touchable tumors were developed on days 6-7. When the tumor volume reached 100 mm³, the tumor-bearing mice were selected for treatment. For laser treatment process, the overlying hair on the tumor was shaved and all mice were anesthetized with a mixture of xylazine and ketamine. The treated mice were kept in separate cages, and tumor volume measurements were made every other day.

NIR Laser Irradiation of Tumors

After tumor volume reached 100 mm³, the tumor-bearing mice were randomly assigned into 5 groups and each group contained 4 mice. These groups include: control group, laser irradiation group, NPs group, NPs + laser irradiation group and NPs + magnet + laser irradiation group. Mice in control and laser irradiation group were injected intravenously with 100 μl of saline. Mice in NPs + laser irradiation group and NPs + magnet + laser irradiation group were injected intravenously with 100 μl of Fe_3O_4@Au NPs (concentration of 150 μg Au/ml). The mice in these two groups were kept for 6 hours for the accumulation of Fe_3O_4@Au NPs in the tumor. The last group was considered for magnetic targeting. In this group, a 3500 Gauss magnet was placed on mice skin in the tumor region. This magnet attracted the Fe_3O_4 core of NPs and accumulated

NPs in the tumor. Then, the tumors were irradiated using an NIR laser (808 nm diode laser) with a laser power density of 2.5 W/cm² for 6 minutes. The day of treatment was day zero. Thereafter, tumor volumes in all mice were measured every other day. Tumor volumes were calculated using this formula [27-29]:

Tumor volume = (π/6×(tumor width)²×(tumor length)

To assess the photothermal therapy efficiency in different groups, the growth inhibition rate (IR) was calculated using the following equation [30, 31]:

$$IR\,(\%) = \left(1 - \left(\frac{V}{V_{control}}\right)\right) \times 100$$

Where V is the average tumor volume in each group, and Control is the average tumor volume in the control group.

To evaluate the toxicity of NPs, the body weight of mice were measured every other day.
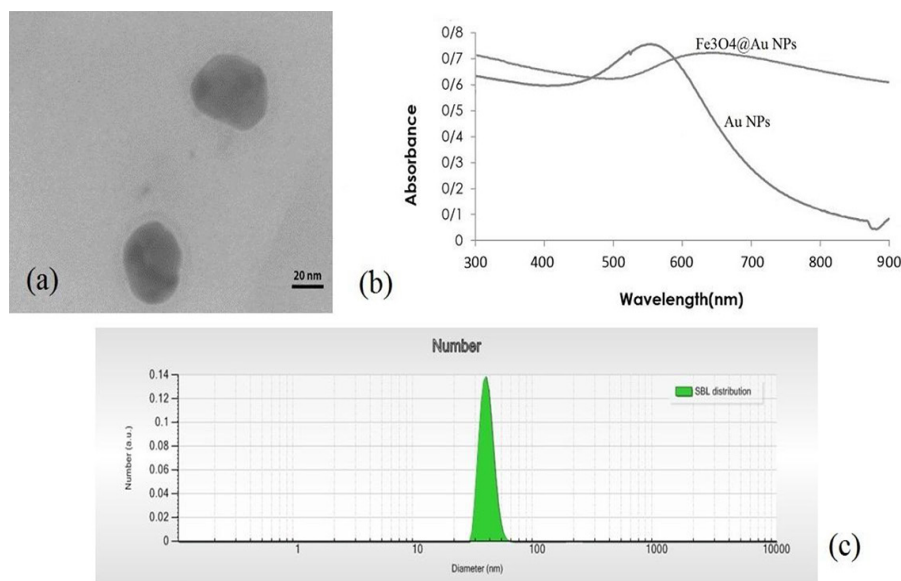
Results

Characterization

Fe_3O_4@Au NPs were successfully synthesized and characterized using TEM, DLS and UV-vis spectroscopy. Figure 1(a) shows a TEM image of Fe_3O_4@Au NPs. The dark region in the center and the peripheral brighter region in the TEM image correspond to Fe3O4 core and Au shell, respectively [32]. As it can be seen from TEM images, Fe_3O_4@Au NPs are approximately spherical. The UV-vis spectroscopic result for these NPs is shown in Figure 1(b). Synthesized Fe_3O_4@Au NPs have an absorption peak at the wavelength of about 650 nm. Figure 1(c) shows the NPs size distribution resulted from DLS analysis. According to Figure 1(c), the effective diameter of Fe_3O_4@Au NPs was approximately 37.8 nm.

Photothermal Conversion of Fe_3O_4@Au NPs Solutions

To evaluate the photothermal effects of Fe_3O_4@Au NPs, the temperature variation of five different concentrations of NPs was mea-

Figure 1: (a) Transmission electron microscopy (TEM) image of Fe$_3$O$_4$@Au nanoparticles (NPs). (b) The absorption spectra of NPs. (c) NPs size distribution resulted from dynamic laser light scattering (DLS).

sured under NIR laser irradiation at four power densities and irradiation time 6 minutes (as described in section photothermal conversion of Fe$_3$O$_4$@Au NPs solutions). The temperature variation for different Au concentrations and different laser power densities are shown in Figure 2.

When these NPs were irradiated using an 808 nm laser, the laser absorbed energy is converted to heat energy that resulted in temperature elevation of NPs solutions (Figure 2). For equal laser power densities, solutions containing Fe$_3$O$_4$@Au NPs achieved higher temperatures compared with PBS samples free of NPs. Laser irradiation with power density of 3.5 W/cm^2 produced average temperature variation of 7.85, 10.20, 12.75, 15.30 and 23.25. When Au concentration was of 0 µg/mL (PBS only), 12.5 µg/mL, 25 µg/mL, 37.5 µg/mL and 50 µg/mL, respectively. For an identical nanoparticle concentration of 50 µg/mL, increasing laser power density resulted in increased temperature variation from 6.9 °C for a power density of 0.9 W/cm^2 to 11.2 °C, 17.9 °C and 23.25°C for power densities of 1.8, 2.5 and 3.5 W/cm^2, respectively.

NIR Laser Irradiation of Tumors

The treatment was performed as mentioned in section NIR laser irradiation of tumors. After treating the mice with described various protocols, the tumor volume in all mice was measured every other day. Figure 3 shows the tumor volume in different groups following the treatment.

As seen in Figure 3, tumor volume in control group increased rapidly while tumor growth in NPs + magnet + laser irradiation group was appropriately controlled. The average tumor volume in control group increased from 105 mm^3 to 4965 mm^3 which was 47.3 times larger than what it was initially. In NPS group, laser irradiation group, NPs + laser irradiation group and NPs + magnet + laser irradiation group, the average tumor volume increased from 103 mm^3 to 4671 mm^3 (45.3 times increase), from 105 mm^3 to 3451 mm^3 (32.8 times increase), from 100 mm^3 to 1993 mm^3 (19.9 times increase) from 99 mm^3 to 768 mm^3 (7.7 times increase), respectively. Skin damage was detected in the NPs + magnet + laser group due to the large temperature change during laser exposure. The damage completely disap-
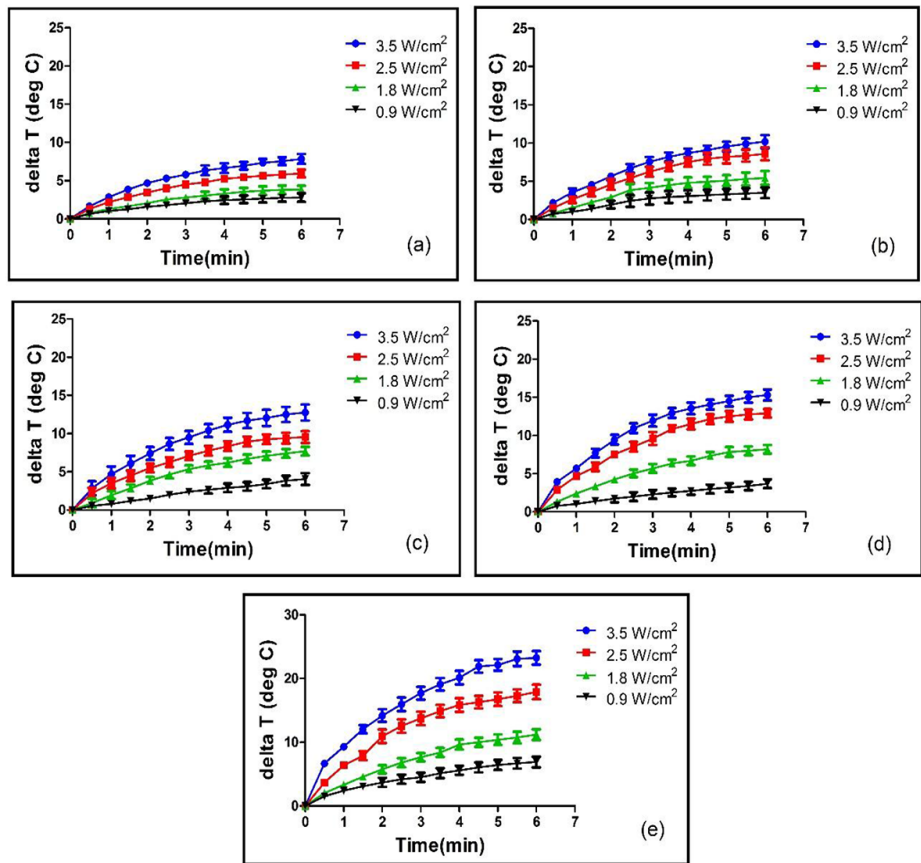
Figure 2: Temperature variation for different Au concentrations and different laser power densities. Figures 2 (a) to (e) correspond to Au concentrations of 0 µg/mL, 12.5 µg/mL, 25 µg/mL, 37.5 µg/mL and 50 µg/mL, respectively.
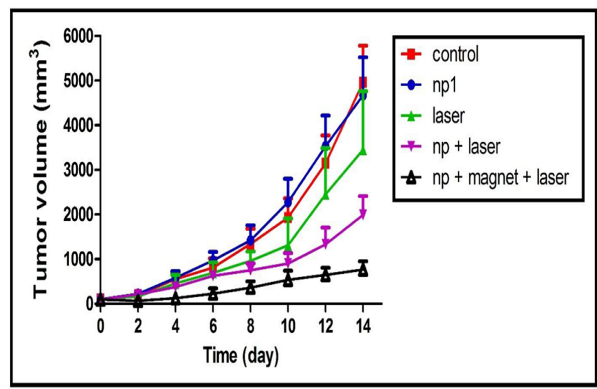

Figure 3: Tumor growth curves vs. time per days after treatment. Various graphs in this figure show the results of control, nanoparticles (NPs), laser, NPs + laser and NPs + magnet + laser groups

peared within two weeks after the treatment.

After 2 weeks post treatment, the average tumor volume in both NPs + laser and NPs + magnet + laser groups was significantly lower than the average of tumor volume in control group (P = 0.028 < 0.05).

The inhibition rate graphs for different groups are depicted in Figure 4. As shown in Figure 4, the inhibition effect of $Fe_3O_4@Au$ NPs + magnet + laser on the tumor was obvious. After the treatment course (2 weeks), the average inhibition rate in NPs + magnet + laser group was 83.5%. The average inhibition rates in NPs group, laser group and NPs + laser group were 6%, 26% and 57%, respectively.

To evaluate the toxicity of NPs, the body weight of mice were measured every other
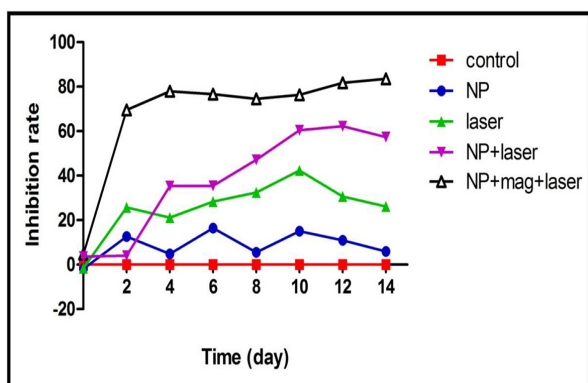
Figure 4: The inhibition rate graphs for different groups of this study. The graphs correspond to control, nanoparticles (NPs), laser, NPs + laser and NPs + magnet + laser groups.
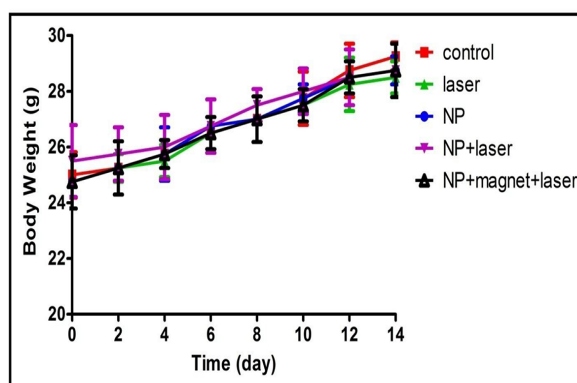
Figure 5: The body weight of mice in different groups. The graphs correspond to control, nanoparticles (NPs), laser, NPs + laser and NPs + magnet + laser groups

day. The body weights of mice in different groups are shown in Figure 5 demonstrating no obvious change in the average body weight for different groups.

Discussion

This study demonstrated the efficacy of using Fe$_3$O$_4$@Au core-shell NPs as a potent photothermal agent for cancer photothermal therapy.

The absorption spectra of Fe$_3$O$_4$@Au NPs, Au and Fe$_3$O$_4$ NPs are shown in Figure 1(b). The absorption peak of 560 nm and 640 nm was observed for Au NPs and Fe$_3$O$_4$@Au NPs, respectively. The absorption peak for Fe$_3$O$_4$@Au NPs showed the peak broadening and a red-shift, which is usually observed in other Au bimetallic core-shell systems [13, 33].

When these NPs were irradiated using an 808 nm laser, the laser absorbed energy is converted to heat energy resulting in temperature elevation of NPs solutions (Figure 2). For equal laser power densities, solutions containing Fe$_3$O$_4$@Au NPs achieved higher temperatures compared with PBS samples without NPs. The temperature variation was both concentration and laser power density dependent. For all power densities at the beginning of laser exposure, the temperature increased

rapidly and then reached a steady state. This pattern of increasing temperature as a result of increasing laser exposure time has been observed by other scientists [34-36].

To evaluate the efficiency of designed treatment protocol, twenty mice were implanted with melanoma cells. The average tumor volume in control group, NPs group, laser irradiation group and NPs + laser irradiation group increased 47.3, 45.3, 32.8 and 19.9 times, respectively. When the magnetic targeting was applied to the NPs + magnet + laser irradiation group, the average tumor volume increased only 7.7 times in 2 weeks. This finding shows that the magnetic targeting in cancer photothermal therapy using Fe$_3$O$_4$@Au NPs resulted in increasing the effectiveness of cancer treatment and tumor growth suppression. Li et al. took advantage of magnetic targeting for remote drug delivery using oligonucleotides-gated silica shell-coated Fe$_3$O$_4$@Au Core-Shell Nanotrisoctahedra and NIR light [22]. Their result indicated that magnetic targeting resulted in NPs accumulation in tumor and the effectiveness of treatment increased.

Two weeks after treatment, the average inhibition rate in NPs + magnet + laser group was 83.5%. The average inhibition rates in NPs group, laser group and NPs + laser group were

6%, 26% and 57%, respectively. Compared to control group, it could be concluded that the inhibition rate of NPs + magnet + laser group was apparent.

For the evaluation of the toxicity of NPs, the body weights of mice were measured every other day (Figure 5). As shown in Figure 5, there was no obvious change in the average body weight in different groups. It should be considered that during two weeks after the treatment day, mice in different groups are able to preserve their body weights (Figure 5), indicating that NPs alone, laser alone, NPs+ laser and NPs + magnet + laser are non-toxic to the mice.

Conclusion

In this study, we synthesized Fe_3O_4@Au core-shell NPs. The super paramagnetic Fe_3O_4 cores can act as magnetic targeting while Au shells function as NIR photothermal therapy converter to ablate tumor tissue. This study indicates the potential of Fe_3O_4@Au NPs in magnetic targeted tissue heating.

Temperature produced by photothermal treatment depends on both NPs concentration and laser power density. The designed treatment protocol in this study destroyed implanted melanoma tumors in C57BL/6 mice. Results show tumor volume in NPs + magnet + laser group was significantly smaller than that of the control group. Therefore, photothermal therapy using Fe_3O_4@Au core-shell NPs is an effective method for cancer treatment.

Acknowledgment

Conflict of Interest

None

References

1. Thompson JF, Scolyer RA, Kefford RF. Cutaneous melanoma in the era of molecular profiling. *Lancet.* 2009;**374**:362-5. doi: 10.1016/S0140-6736(09)61397-0. PubMed PMID: 19647595.

2. Huo L, Yao H, Wang X, Wong GW, Kung HF, Lin MC. Inhibition of melanoma growth by subcutaneous administration of hTERTC27 viral cocktail in C57BL/6 mice. *PLoS One.* 2010;**5**:e12705. doi: 10.1371/journal.pone.0012705. PubMed PMID: 20856939. PubMed PMCID: PMC2938346.

3. Doaga A. Phenomenological study of thermal field generated by nanoparticles arrays in hypertermia as treatment method. *Journal of Advanced Research in Physics.* 2011;**2**.

4. Beik J, Abed Z, Shakeri-Zadeh A, Nourbakhsh M, Shiran MB. Evaluation of the sonosensitizing properties of nano-graphene oxide in comparison with iron oxide and gold nanoparticles. *Physica E Low Dimens Syst Nanostruct.* 2016;**81**:308-14.

5. Niemz MH. Laser-tissue interactions: fundamentals and applications. Berlin: Springer Science & Business Media; 2013. p. 303.

6. Neshastehriz A, Tabei M, Maleki S, Eynali S, Shakeri-Zadeh A. Photothermal therapy using folate conjugated gold nanoparticles enhances the effects of 6 MV X-ray on mouth epidermal carcinoma cells. *JJ Photochem Photobiol B.* 2017;**172**:52-60.

7. O'Neal DP, Hirsch LR, Halas NJ, Payne JD, West JL. Photo-thermal tumor ablation in mice using near infrared-absorbing nanoparticles. *Cancer Lett.* 2004;**209**:171-6. doi: 10.1016/j.canlet.2004.02.004. PubMed PMID: 15159019.

8. Sayed IH, Huang X, El-Sayed MA. Selective laser photo-thermal therapy of epithelial carcinoma using anti-EGFR antibody conjugated gold nanoparticles. *Cancer Lett.* 2006;**239**:129-35. doi: 10.1016/j.canlet.2005.07.035. PubMed PMID: 16198049.

9. Heidari M, Sattarahmady N, Azarpira N, Heli H, Mehdizadeh AR, Zare T. Photothermal cancer therapy by gold-ferrite nanocomposite and near-infrared laser in animal model. *Lasers Med Sci.* 2016;**31**:221-7. doi: 10.1007/s10103-015-1847-x. PubMed PMID: 26694488.

10. Robinson DS, Parel JM, Denham DB, Gonzalez-Cirre X, Manns F, Milne PJ, et al. Interstitial laser hyperthermia model development for minimally invasive therapy of breast carcinoma. *J Am Coll Surg.* 1998;**186**:284-92. PubMed PMID: 9510259.

11. Masters A, Steger AC, Lees WR, Walmsley KM, Bown SG. Interstitial laser hyperthermia: a new approach for treating liver metastases. *Br J Cancer.* 1992;**66**:518-22. PubMed PMID: 1520588. PubMed PMCID: PMC1977951.

12. Park JH, Von Maltzahn G, Xu MJ, Fogal V, Kotamraju VR, Ruoslahti E, et al. Cooperative nanomaterial system to sensitize, target, and treat tumors. *Proc Natl Acad Sci U S A.* 2010;**107**:981-6.

doi: 10.1073/pnas.0909565107. PubMed PMID: 20080556. PubMed PMCID: PMC2824295.

13. Guo Y, Zhang Z, Kim DH, Li W, Nicolai J, Procissi D, et al. Photothermal ablation of pancreatic cancer cells with hybrid iron-oxide core gold-shell nanoparticles. *Int J Nanomedicine.* 2013;**8**:3437-46. doi: 10.2147/IJN.S47585. PubMed PMID: 24039426. PubMed PMCID: PMC3771851.

14. Zharov V, Letfullin R, Galitovskaya E. Microbubbles-overlapping mode for laser killing of cancer cells with absorbing nanoparticle clusters. *Journal of Physics D: Applied Physics.* 2005;**38**:2571.

15. Jain PK, Lee KS, El-Sayed IH, El-Sayed MA. Calculated absorption and scattering properties of gold nanoparticles of different size, shape, and composition: applications in biological imaging and biomedicine. *J Phys Chem B.* 2006;**110**:7238-48. doi: 10.1021/jp057170o. PubMed PMID: 16599493.

16. Huang X, El-Sayed MA. Gold nanoparticles: optical properties and implementations in cancer diagnosis and photothermal therapy. *Journal of Advanced Research.* 2010;**1**:13-28.

17. Pedrosa P, Vinhas R, Fernandes A, Baptista PV. Gold Nanotheranostics: Proof-of-Concept or Clinical Tool? *Nanomaterials (Basel).* 2015;**5**:1853-79. doi: 10.3390/nano5041853. PubMed PMID: 28347100. PubMed PMCID: PMC5304792.

18. Wang X, Liu H, Chen D, Meng X, Liu T, Fu C, et al. Multifunctional Fe₃O₄@P(St/MAA)@chitosan@Au core/shell nanoparticles for dual imaging and photothermal therapy. *ACS Appl Mater Interfaces.* 2013;**5**:4966-71. doi: 10.1021/am400721s. PubMed PMID: 23683167.

19. Li C, Chen T, Ocsoy I, Zhu G, Yasun E, You M, et al. Gold?Coated Fe3O4 Nanoroses with Five Unique Functions for Cancer Cell Targeting, Imaging, and Therapy. *Advanced Functional Materials.* 2014;**24**:1772-80.

20. Feng W, Zhou X, Nie W, Chen L, Qiu K, Zhang Y, et al. Au/polypyrrole@Fe3O4 nanocomposites for MR/CT dual-modal imaging guided-photothermal therapy: an in vitro study. *ACS Appl Mater Interfaces.* 2015;**7**:4354-67. doi: 10.1021/am508837v. PubMed PMID: 25664659.

21. Hu Y, Meng L, Niu L, Lu Q. Facile synthesis of superparamagnetic Fe3O4@polyphosphazene@Au shells for magnetic resonance imaging and photothermal therapy. *ACS Appl Mater Interfaces.* 2013;**5**:4586-91. doi: 10.1021/am400843d. PubMed PMID: 23659588.

22. Li WP, Liao PY, Su CH, Yeh CS. Formation of oligonucleotide-gated silica shell-coated Fe(3)O(4)-Au core-shell nanotrisoctahedra for magnetically targeted and near-infrared light-responsive theranostic platform. *J Am Chem Soc.* 2014;**136**:10062-75. doi: 10.1021/ja504118q. PubMed PMID: 24953310.

23. Hoskins C, Min Y, Gueorguieva M, McDougall C, Volovick A, Prentice P, et al. Hybrid gold-iron oxide nanoparticles as a multifunctional platform for biomedical application. *J Nanobiotechnology.* 2012;**10**:27. doi: 10.1186/1477-3155-10-27. PubMed PMID: 22731703. PubMed PMCID: PMC3448509.

24. Montazerabadi AR, Oghabian MA, Irajirad R, Muhammadnejad S, Ahmadvand D, Delavari H H, et al. Development of gold-coated magnetic nanoparticles as a potential MRI contrast agent. *Nano.* 2015;**10**:1550048.

25. Massart R. Preparation of aqueous magnetic liquids in alkaline and acidic media. *IEEE transactions on magnetics.* 1981;**17**:1247-8.

26. Jana NR, Gearheart L, Murphy CJ. Seeding growth for size control of 5? 40 nm diameter gold nanoparticles. *Langmuir.* 2001;**17**:6782-6.

27. Jensen MM, Jørgensen JT, Binderup T, Kjær A. Tumor volume in subcutaneous mouse xenografts measured by microCT is more accurate and reproducible than determined by 18 F-FDG-microPET or external caliper. *BMC Med Imaging.* 2008;**8**:16.

28. Cheng L, Yang K, Li Y, Zeng X, Shao M, Lee ST, et al. Multifunctional nanoparticles for upconversion luminescence/MR multimodal imaging and magnetically targeted photothermal therapy. *Biomaterials.* 2012;**33**:2215-22. doi: 10.1016/j.biomaterials.2011.11.069. PubMed PMID: 22169825.

29. Kersemans V, Cornelissen B, Allen PD, Beech JS, Smart SC. Subcutaneous tumor volume measurement in the awake, manually restrained mouse using MRI. *J Magn Reson Imaging.* 2013;**37**:1499-504. doi: 10.1002/jmri.23829. PubMed PMID: 23023925.

30. Liu H, Chen D, Tang F, Du G, Li L, Meng X, et al. Photothermal therapy of Lewis lung carcinoma in mice using gold nanoshells on carboxylated polystyrene spheres. *Nanotechnology.* 2008;**19**:455101. doi: 10.1088/0957-4484/19/45/455101. PubMed PMID: 21832760.

31. Yan LL, Zhang YJ, Gao WY, Man SL, Wang Y. In vitro and in vivo anticancer activity of steroid saponins of Paris polyphylla var. yunnanensis. *Exp Oncol.* 2009;**31**:27-32. PubMed PMID: 19300413.

32. Robinson I, Tung LD, Maenosono S, Walti C, Thanh NT. Synthesis of core-shell gold coated magnetic nanoparticles and their interaction with thiolated DNA. *Nanoscale.* 2010;**2**:2624-30. doi: 10.1039/

c0nr00621a. PubMed PMID: 20967339.

33. Lyon JL, Fleming DA, Stone MB, Schiffer P, Williams ME. Synthesis of Fe oxide core/Au shell nanoparticles by iterative hydroxylamine seeding. *Nano Letters*. 2004;**4**:719-23.

34. Cheong SK, Krishnan S, Cho SH. Modeling of plasmonic heating from individual gold nanoshells for near-infrared laser-induced thermal therapy. *Med Phys*. 2009;**36**:4664-71. doi: 10.1118/1.3215536. PubMed PMID: 19928098.

35. Elliott AM, Shetty AM, Wang J, Hazle JD, Jason Stafford R. Use of gold nanoshells to constrain and enhance laser thermal therapy of metastatic liver tumours. *Int J Hyperthermia*. 2010;**26**:434-40. doi: 10.3109/02656731003685805. PubMed PMID: 20597626.

36. Elliott AM, Stafford RJ, Schwartz J, Wang J, Shetty AM, Bourgoyne C, et al. Laser-induced thermal response and characterization of nanoparticles for cancer treatment using magnetic resonance thermal imaging. *Med Phys*. 2007;**34**:3102-8. doi: 10.1118/1.2733801. PubMed PMID: 17822017.